Biophysical Journal, Volume *113*

Supplemental Information

Adaptive Response of Actin Bundles under Mechanical Stress

Florian Rückerl, Martin Lenz, Timo Betz, John Manzi, Jean-Louis Martiel, Mahassine Safouane, Rajaa Paterski-Boujemaa, Laurent Blanchoin, and Cécile Sykes

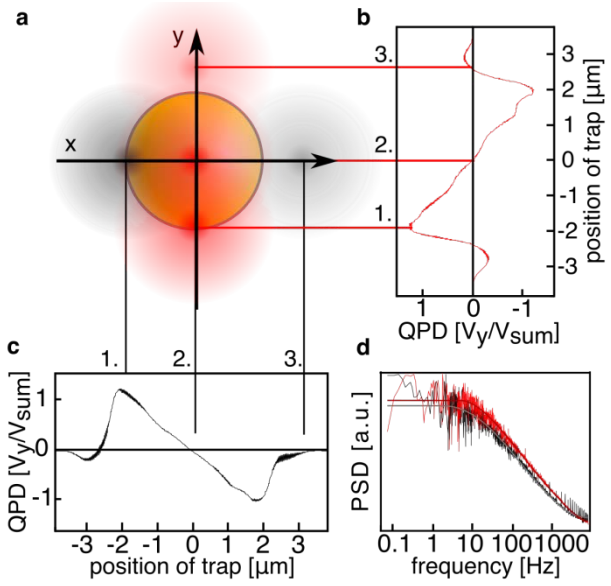

Figure S1: Schematic of trap calibration using time-shared multiple optical traps. (a) Illustration of the scanning motion of the traps. The intensity of the laser traps is collected by a four quadrant diode (QPD), allowing to determine the displacement of the bead in the trap. (b) and (c) Normalized voltage signal on the QPD in x- and y-direction (red and black curve, respectively). The linear region around the center is used to convert the recorded signal into the displacement of the bead in trap. The numbers 1-3 indicate the different positions of the trap with respect to the bead, and the corresponding signal on the QPD. (d) Power spectral density (PSD) calculated from the thermal motion of the bead in the trap. From these curves the trap stiffness is obtained in x- and y-direction following the procedure described by Berg-Sørensen and Flyvbjerg (1).

Figure S2: Time traces of several compression-expansion experiments at different speeds. (a)-(f) corresponds to trap velocities of 0.5, 1, 2, 5, 10, and 20 μm/s, respectively. All curves show similar features, namely a distinct buckling event in the first compression phase and a high degree of uniformity in the following cycles, indicating that the bundle reaches a steady state. Note that the model does not reproduce the initial sharp peak in the force curve in the three fastest compression experiments, suggesting that they may involve additional irreversible mechanisms, e.g., filament breaking. Red curves correspond to the fit described in the main text of the paper. Each curve corresponds to a different bundle, and one set of parameters τ, k_s and κ is used to fit each curve (see Table S1).

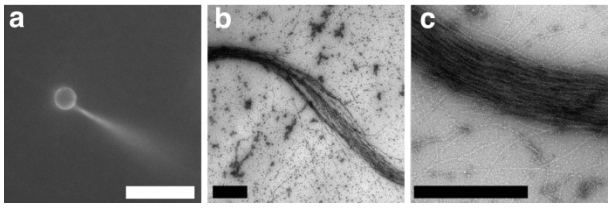

Figure S3: Fluorescent and electron microscopy images of actin bundles. (a) A typical image of a single bundle protruding from a mDia1 coated latex bead (d=2µm), the scale bar is 10µm. (b-c) EM micrographs of an actin bundle. The average thickness of the bundle grown in solution (for details on the buffer see Materials and Methods) is estimated to be between 200 and 700nm. The scale bar is 1µm in both (b) and (c).

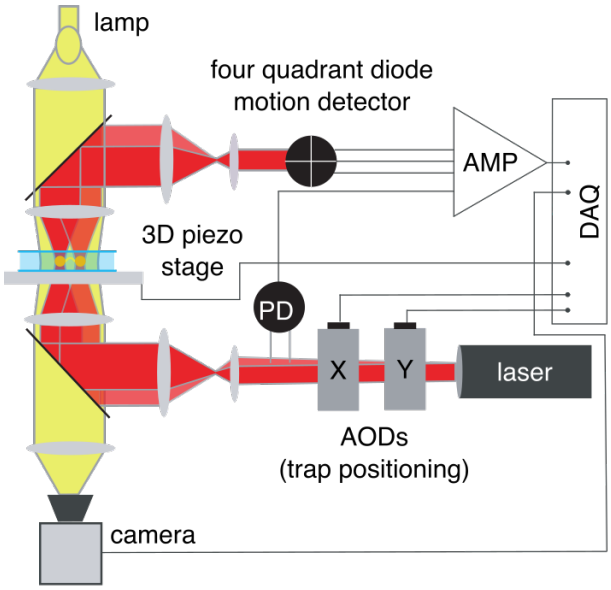

Figure S4: Schematic of the multiple optical tweezer setup. The position of the traps in the object plane is controlled by passing the IR through two computer controlled and perpendicularly oriented acousto-optical deflectors (AODs). Then the beam is widened to slightly overfill the back aperture of the focusing objective and the light is collected by a long distance objective. Positioning of the sample is achieved by a 3D piezo stage. The position of trapped beads is detected using a four-quadrant photo diode (QPD), connected to an amplifier. Two controller cards from National Instruments are used for data acquisition and setup control, allowing a sampling rate of 500kHz per channel of the QPD.

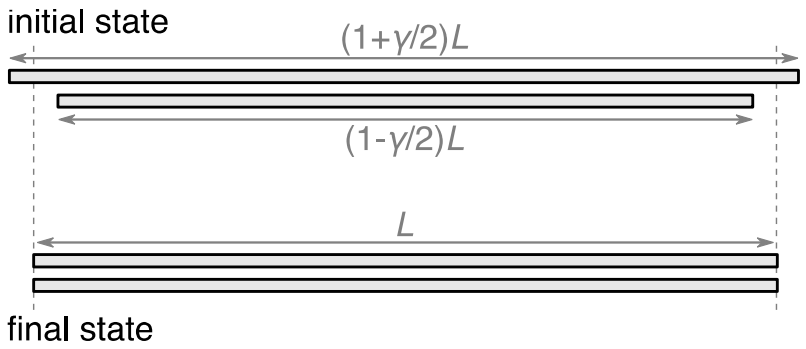

Figure S5: Minimal geometry for the relaxation of an inter-bundle strain. In the initial state, the top filament is stretched with a strain $\gamma/2$, while the bottom filament is compressed with a strain $-\gamma/2$. As discussed in the Supplemental text, the viscoelastic time τ is the characteristic time associated to the relaxation of the small relative strain γ.

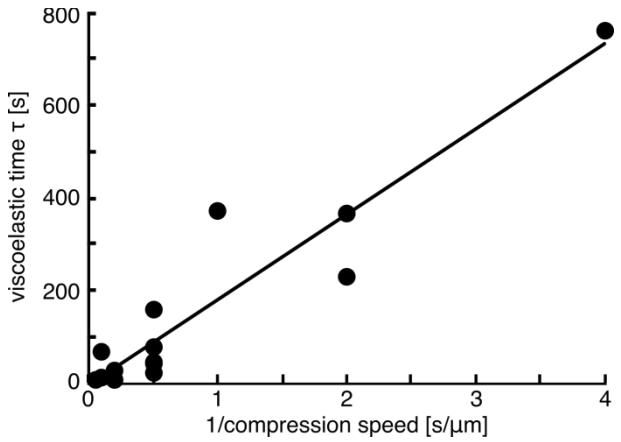

Figure S6: Dependency of the characteristic viscous time on compression speed, taken from the values of Table 1. Note that the viscoelastic time is obtained by fitting the experimental data with the model described in the main text. Pointing at further underlying complexity of the system. The line is a guide for the eye, illustrating the apparent proportionality between the viscoelastic time τ and the inverse compression speed.

Table S1 Parameters from the fits of data without waiting times, using the model described in the main text of the article. T is the driving period, L_0 the initial length of the bundle, κ the bending modulus, k_s the stretching modulus, and τ the viscoelastic time. The line with the asterisk indicates the data shown in Fig. 2. Note that each data set corresponds to a different bundle.

Trap speed [μm/s]	T [s]	L_0 [μm]	κ [pN μm^2]	k_S [pN]	τ [s]	Max. Strain
0.25	40.0	36.93	1179.4	64.4	765.6	0.117
0.5	80.0	30.29	344.2	19.0	231.4	0.613
0.5	80.0	34.91	299.8	51.8	370.4	0.548
*1.0	40.0	34.92	687.9	54.3	375.5	0.527
2.0	20.0	34.93	302.1	85.3	42.8	0.548
2.0	20.0	34.91	426.9	114.6	77.5	0.544
2.0	20.0	34.96	689.3	72.2	161.8	0.528
2.0	8.0	36.93	747.4	168.7	46.0	0.187
2.0	5.0	36.92	871.7	254.8	24.5	0.106
5.0	8.0	33.03	637.4	174.9	22.7	0.542
5.0	8.0	34.93	461.6	141.7	30.0	0.540
5.0	2.0	36.94	1785.3	174.9	9.5	0.101
10.0	4.0	34.96	574.4	202.5	13.1	0.530
10.0	4.0	34.95	2175.1	31.9	68.7	0.469
20.0	2.0	34.97	695.8	233.8	6.7	0.509

Supplemental Information

Fitting of the viscoelastic model to experimental data

To determine the bundle's viscoelastic parameters, we fit the model described in equations [1-3] (see main text) to the experimentally obtained force curves [*e.g.*, that of Fig. 2a]. We substitute the expressions of σ_L, σ_θ and f from equations [2] and [3] into equation [1] to obtain a system of two nonlinear differential equations for two unknown functions $L(t)$ and $\theta(t)$. We solve this system numerically using Mathematica's numerical differential equation solver while driving the model with a function $X(t)$ (representing the distance between the centers of the two optical traps) identical to that used in the experiment. We then use equation [3] to compute the function $f(t)$ from the solutions $L(t)$ and $\theta(t)$, and compute the mean square distance between $f(t)$ and the measured experimental force curve. We repeat the operation to minimize this mean square distance over experimental parameters k_s, κ and τ according to Mathematica's derivative-free principal axis method (2).

Estimate of the number of filaments in the bundle and if they are weakly or strongly coupled

The buckling force F_B of a bundle made out of N filaments of initial length L_0 is given by (3):

$$F_B = \frac{\pi^2 k_B T L_p}{L_0^2} = \frac{\pi^2 k_B T N^c l_p}{L_0^2}, \qquad [4]$$

where $L_p = \kappa/k_B T$ is the persistence length of the bundle, l_p the persistence length of a single actin filament. The exponent c varies between 1 and 2 depending on whether the filaments are weakly ($c = 1$), or strongly ($c = 2$) coupled (4). In the strongly-coupled limit, the filaments are held in register with respect to each other, similar to rows of atoms in a single metallic beam. Conversely, in a weakly

coupled bundle, filaments may come out of register, and the bending rigidity of the beam is the sum of those of the filaments, with no dramatic contribution from the couplings. Previous reports show that c approaches 2 for bundles stabilized by depletion agents (4).

To assess whether the internal bundle mechanics probed here is more consistent with weak or strong interactions, we use equation [4] to infer the typical number of filaments in our bundle from our measurement of its bending modulus as $N = (\kappa/k_B T l_p)^{1/c}$. Using our measured average $\kappa \simeq 770$ pN $\cdot$ μm^2 and the value $l_p \simeq 10$ μm, we consider the two extreme cases of strong interactions ($c = 2$), and weak interactions ($c = 1$), yielding $N_{c=2} \simeq 140$, and $N_{c=1} \simeq 19{,}000$, respectively. These widely different estimates, are consistent with widely different bundle radii: the strong binding hypothesis should yield a relatively thin bundle with radius $r_{\mathrm{bundle}} \simeq r_{\mathrm{F-actin}}\sqrt{N_{c=2}} \simeq 35$ nm, where we used $r_{\mathrm{F-actin}} \simeq 3$ nm for the radius of a single actin filament. On the other hand, the weak binding hypothesis implies a much thicker bundle radius $r_{\mathrm{bundle}} \simeq r_{\mathrm{F-actin}}\sqrt{N_{c=1}} \simeq 420$ nm.

These values correspond to a bundle thickness of $r_{\mathrm{bundle}} \simeq r_{\mathrm{F-actin}}\sqrt{N_{c=2}} = 35 \pm 4$ nm and $r_{\mathrm{bundle}} \simeq r_{\mathrm{F-actin}}\sqrt{N_{c=1}} = 416 \pm 94$ nm, respectively, in agreement with the above estimates from the model. We discriminate between these two hypotheses through direct inspection of the bundles in electron microscopy, which reveal a bundle diameter $r_{\mathrm{bundle}} \simeq 200 - 700$ nm (see supplemental Fig. S3). We conclude that filaments within the bundle are weakly coupled.

Inter-filament friction coefficient estimate

To compare the magnitude of the friction in our experiments and in Ref. (5), we compute and orders of magnitude for the friction coefficients associated with each study. We first consider two filaments that

translate relative to each other with a uniform velocity v, and define the friction coefficient ζ between two filaments through

$$f = -\zeta L v, \qquad [5]$$

where L is the length of the overlap between the two filaments, and f is the friction force between them. The viscoelastic relaxation time τ introduced in the main text is the typical time required to relax a differential stretching between the two filaments in the presence of such a friction, as illustrated in Fig. S5. In the configuration considered, the elastic energy associated to either one of the filaments reads

$$E = \frac{k_s}{2}\left(\frac{\gamma}{2}\right)^2, \qquad [6]$$

while the power dissipated at the interface between the two filaments is the work performed by the friction force f, namely

$$P = \int_{-L/2}^{L/2} \zeta\, v(s)^2 \, \mathrm{d}s, \qquad [7]$$

where $v(s)$ denotes the (non-uniform) relative velocity between the two filaments at the curvilinear coordinate s. As the present calculation only intends to provide an order-of-magnitude estimate of the bundle viscoelastic time, in the following we use the simplifying assumption that filaments deform affinely, implying $v(s) = s\frac{\mathrm{d}\gamma}{\mathrm{d}t}$ to first order in γ.

Let us now consider a full close-packed bundle, where each filament has six neighbors with mismatched lengths. In such a situation, there are three times as many filament-filament interfaces as there are filaments. Balancing the power dissipated through friction with the change in elastic energy of the bundle, we thus obtain

$$\frac{\mathrm{d}E}{\mathrm{d}t} = -3P. \qquad [8]$$

Inserting the expressions of E and P into this equation, we find that the strain γ evolves according to:

$$\frac{\mathrm{d}\gamma}{\mathrm{d}t} = -\frac{8k_s}{\zeta L^2}\gamma, \qquad [9]$$

implying an exponential relaxation with viscoelastic time

$$\tau = \frac{\zeta L^2}{8k_s}. \qquad [10]$$

Using the average values measured in our study, namely $k_s = 120$ pN, $\tau = 150$ s and $L = 35$ µm, we invert this relation to compute an inter-filament friction coefficient $\zeta \simeq 117\ \mathrm{N \cdot s \cdot m^{-2}}$. By comparison, Ref. (5) reports typical friction forces of the order of $f = 5$ pN for filaments overlapping over a length $L = 2$ µm and sliding at speeds $v = 100\ \mathrm{nm \cdot s^{-1}}$, yielding a friction coefficient of the order of $\zeta \simeq 25\ \mathrm{N \cdot s \cdot m^{-2}}$. Despite the substantial differences in geometry and confinement of the filaments, it thus appears that the frictional forces encountered in our study are of the same order of magnitude as those previously reported in Ref. (5).

Variability of the characteristic viscoelastic time τ

While the short-time, elastic properties of the bundle are well-explained by combining the known elastic characteristics of individual filaments with a weak-binding hypothesis, their viscoelastic behavior proves to be more complex. In classical Maxwell models the viscoelastic time of the material is a material property independent on the frequency at which it is driven. In contrast, we show in Fig. S5 that in our bundles, the parameter τ appears to decrease with increasing driving frequency, *i.e.*, a higher compression speed. Assuming that the critical strain required for buckling is similar in all experiments presented in Fig. S2, the time to reach it (the visco-elastic time) is inversely proportional to the bundle compression velocity.

Bibliography:

1. Berg-Sørensen, K., and H. Flyvbjerg. 2004. Power spectrum analysis for optical tweezers. Review of Scientific Instruments 75:594-612.
2. Brent, R. P. 1973. Algorithms for minimization without derivatives. Prentice Hall (reprinted by Dover, 2002 and 2013).
3. Landau, L. D., L. P. Pitaevskii, A. M. Kosevich, and E. M. Lifshitz. 2012. Theory of Elasticity. In 123Library. Butterworth-Heinemann.
4. Claessens, M. M., M. Bathe, E. Frey, and A. R. Bausch. 2006. Actin-binding proteins sensitively mediate F-actin bundle stiffness. Nat Mater 5:748-753.
5. Ward, A., F. Hilitski, W. Schwenger, D. Welch, A. W. Lau, V. Vitelli, L. Mahadevan, and Z. Dogic. 2015. Solid friction between soft filaments. Nat Mater 14:583-588.